Creation and Destruction of Skyrmions via Electrical Modulation of Local Magnetic Anisotropy in Magnetic Thin Films

Xinyi Xu, Xi-Lai Li, Yuriy G. Semenov, and Ki Wook Kim

Creation and Destruction of Skyrmions via Electrical Modulation of Local Magnetic Anisotropy in Magnetic Thin Films

Xinyi Xu,[1] Xi-Lai Li,[1] Yuriy G. Semenov,[1] and Ki Wook Kim[1,2,*]

[1]Department of Electrical and Computer Engineering,

North Carolina State University, Raleigh, NC 27695, USA

[2]Department of Physics, North Carolina State University, Raleigh, NC 27695, USA[*]

Abstract

Formation and dissolution of skyrmions via local modulation of magnetic anisotropy is theoretically explored in ferromagnetic (FM) and antiferromagnetic (AFM) thin-film structures. Using a micromagnetic simulation, the spatial and temporal evolution of spin textures are analyzed while the effect of externally controlled effective magnetic anisotropy is introduced for a finite duration. Simulation results clearly indicate that the Néel-type skyrmions can be excited and destroyed in a FM or an AFM layer in selected parameter windows, enabling deterministic encoding of logical states "1" and "0" in this physical system. The characteristic times for the dynamical responses are much faster in the AFMs, particularly in the creation process. The size of the excitation region can be scaled down to the sub-10 nm range in the radius. The investigation also examines the effect of inhomogeneous in-plane magnetic properties, further elucidating the feasibility in realistic conditions. Considering the low power and locally controlled nature of magnetic anisotropy modulation, this approach is expected to provide a highly efficient means for achieving skyrmion based devices. The AFMs offer a particularly promising opportunity.

PACS numbers:

---

[*]Electronic address: kwk@ncsu.edu

I.   INTRODUCTION

The concept of skyrmion, a particle-like topological soliton first introduced to explain hadrons [1], has recently been extended to a nanoscale local whirl of spin textures in a magnetic material [2]. In this magnetic adaptation, a skyrmion has its magnetization at the core aligned antiparallel to the background orientation which is surrounded by an axially symmetric twist bringing the two oppositive configurations together with the aid of the Dzyaloshinskii-Moriya interaction (DMI). Similar to the domain walls, it can be categorized into two different types (e.g., Bloch and Néel skyrmions) depending on whether the spins rotate in the tangential planes perpendicular to the radial direction or in the radial planes when moving from the core to the periphery. Since then, the topologically protected nature of magnetic skyrmions even at the nanometer scale has brought significant attention as a carrier of information for computing and storage beyond the CMOS based systems [3, 4]. A number of experimental and theoretical investigations have already demonstrated the possibility of controlling individual skyrmion in bulk and thin film, including skyrmion generation, transfer, and deletion via magnetic fields [5], local heating [6, 7], spin-polarized current [8–10], and other mechanisms such as topological transitions [11–18].

While skyrmion creation by an electrical current (in a geometrically constricted structure) was a particularly critical achievement [11], a mechanism that enables local excitation and destruction can offer more versatility in the applications. At the same time, an electrostatic approach can be more energy efficient than those based on the current driven methods [11–13]. Modulation of magnetic anisotropy via the magnetoelectric effect may allow the desired possibility for it is one of the key parameters in the skyrmion dynamics. As it is well known, magnetic anisotropy at the interface between a thin magnetic film and a nonmagnetic material depends sensitively on the electric field applied to the layered structure. For instance, a simple exchange of the anode and the cathode (i.e., the polarity of the bias voltage) can significantly alter the perpendicular component of the anisotropy by either enhancing or suppressing it in the magnet [19, 20]. This local manipulation of perpendicular magnetic anisotropy (PMA), known conveniently as the voltage controlled magnetic anisotropy (VCMA), can lead to anisotropy-driven magnetization rotation [20–22] potentially altering the spin textures without current dissipation. In fact, the induced effective magnetic field was shown theoretically to enable efficient skyrmion transfer on the thin-film plane [23–25]

2

as well as core reversal in a pillar geometry [26]. The effect of VCMA itself has been studied extensively in both ferromagnetic (FM) and antiferromagnetic (AFM) materials with a large change in the anisotropy field demonstrated in the literature [19, 20, 27–30].

In this work, we theoretically explore generation and destruction of skyrmions via local modulation of magnetic anisotropy (such as VCMA) in a magnetic thin-film structure. The magnetization dynamics is analyzed by numerically solving the Landau-Lifshitz-Gilbert (LLG) equation based on Object Oriented MicroMagnetic Framework (OOMMF) [31]. Simulation results clearly indicate that the Néel-type skyrmions can be excited and destroyed in a FM or an AFM layer as desired. Thus, it appears possible to write logical states "1" and "0" (e.g., the presence and absence of a skyrmion) deterministically with properly selected materials and other relevant parameters. The characteristic time for generation is estimated to be around 1 ns and a few ps for the FM and AFM, respectively, while the destruction can be much faster (in the range of ∼15 ps and ∼2 ps, respectively). The size of the excitation can reach the sub-10 nm scale in the radius as well. Our investigation also examines the effect of inhomogeneous in-plane magnetic properties, further elucidating the feasibility in realistic applications.

II.   THEORETICAL MODEL

A schematic of the structure under consideration is shown in Fig. 1. It resembles a racetrack-like device [32, 33], where the information can be written on the magnetic carrier (i.e., skyrmion creation and destruction in this case), transferred or stored along the channel, and read when necessary. The combination of a magnetic thin film (FM or AFM) and a spin-orbit coupled material (such as heavy metals and topological insulators) allow skyrmion excitation as well as its back and forth movement via the spin-orbit torque as discussed in the literature [10, 12, 34, 35]. In particular, the AFM skyrmions are expected to move straight along the driving current due to the cancellation of the Magnus force unlike the FM counterparts [12, 35]. Detection of skyrmion presence (and thus absence) can be achieved via the non-colinear magnetoresistance in a magnetic tunnel junction (MTJ) geometry by taking advantage of the non-uniform spin textures of the skyrmion [36].

For a quantitative evaluation, the magnetic film is assumed to be 1 nm thick with the easy axis along the vertical z direction. The cross-plane magnetic anisotropy K_z is set

at 200 kJ/m^3, while those in the thin-film plane are initially taken to be $K_x = K_y = 0$ followed by the consideration of complex conditions with unequal values (i.e., $K_x \neq K_y$). The saturation magnetization M_s of 160 kA/m and the Gilbert damping constant α of 0.05 for the FM and 0.01 for the AFM are adopted, respectively. The change in the magnetic anisotropy profile (i.e., strengthening or weakening the PMA) induced by the applied bias is assumed to be limited to the region directly beneath the gate. For convenience, the gate electrode is taken to have a circular shape with the radius of 15 nm. Beside the VCMA, note that a similar change in the magnetic anisotropy can also be achieved by the magnetoelastic effect [37]. In the latter case, a piezoelectric insulator is needed in place of a normal dielectric. The magnetization (or the Néel vector) of the magnetic layer is aligned uniformly along the $+\hat{\mathbf{z}}$ direction at the start. The discussion hereinafter is focused only on the "write" mechanism−both logical states "1" and "0".

A micromagnetic model is adopted to fully analyze spatial and temporal dynamics as mentioned above [31]. The effective magnetic field necessary for the LLG simulation can be obtained from the magnetic energy or Hamiltonian H as $H_{\text{eff}} = -(\partial H / \partial \mathbf{m})$. In the calculation, the DMI is taken into consideration as well as the exchange interaction and anisotropy energy. The Zeeman energy term is neglected since the external magnetic field is not considered. Accordingly, the Hamiltonian for the FM case can be written as

$$H_{\text{FM}} = A \sum_{<i,j>} \mathbf{m}_i \cdot \mathbf{m}_j + \sum_{<i,j>} \mathbf{D} \cdot (\mathbf{m}_i \times \mathbf{m}_j) - K \sum_i m_{i,z}^2, \tag{1}$$

where $\mathbf{m}_i$ represents the normalized local magnetic moment (i.e., $|\mathbf{m}_i| = 1$) and i, j runs over all of the nearest neighbor cells. In addition, A and K denote the exchange stiffness and anisotropy constant (z component), respectively, whereas $\mathbf{D}$ is the DMI vector [12]. Note that the term K accounts for the contribution of the biased induced PMA (K_{pma}) when the signal pulse is applied (i.e., $K = K_z + K_{\text{pma}}$). For the AFM structure, $\mathbf{m}_A$ and $\mathbf{m}_B$ are substituted by $\mathbf{n}_A$ and $\mathbf{n}_B$ (with $\mathbf{n}_A = \mathbf{m}_A$ and $\mathbf{n}_B = -\mathbf{m}_B$). Then, the corresponding expression becomes

$$H_{\text{AFM}} = -A \sum_{<i,j>} \mathbf{n}_i \cdot \mathbf{n}_j - \sum_{<i,j>} \mathbf{D} \cdot (\mathbf{n}_i \times \mathbf{n}_j) - K \sum_i n_{i,z}^2. \tag{2}$$

By convention, A and the DMI constant D take negative values for the AFM calculation [12, 35].

III. RESULTS AND DISCUSSION

Figure 2 shows representative snapshots of the simulated spin texture evolution in both FM and AFM films, highlighting skyrmion formation and dissolution. For generation, the applied bias pulse is assumed to introduce a negative component in the PMA ($K_{\text{pma}} = -400 \, \text{kJ/m}^3$) for a duration Δt of 100 ps (FM) and 1 ps (AFM), respectively. By switching the magnet to be with easy-plane anisotropy (x-y) under the gate, the spins within the affected region rotate toward the in-plane direction, followed by the core proceeding to the antiparallel side (i.e., $m_z < 0$) with the induced field-like torque. The resulting texture is similar to that of a skyrmion but unstable. Only after the bias pulse cedes, the spins at the core and the surrounding area relax gradually (with some oscillatory motions) to an equilibrium state with a whirl configuration. The observed skyrmion formation takes about 1 ns for FM and $\sim$10 ps for AFM, depending on α and the PMA pulse. It is also interesting to learn that the actual dimension of the gate doesn't appear to have any discernible impact on the size/stability of the created skyrmions so long as it is varied in the comparable range. On the other hand, the process tends to take a longer time with a smaller excitation region. To dissolve a skyrmion, a bias pulse that strengthens the PMA is required in contrast. Then, the affected skymion shrinks in size until it disappears completely. With $K_{\text{pma}} = +100 \, \text{kJ/m}^3$ and the pulse duration Δt of 20 ps, a FM skyrmion is deleted in $\sim$15 ps. In comparison, AFM skyrmions need a much shorter Δt of $\sim$1.5 ps. In the calculation, $A = 5 \, \text{pJ/m}$, $D = 1.2 \, \text{mJ/m}^2$ are used for the FM structure whereas it is $A = -3 \, \text{pJ/m}$, $D = -0.9 \, \text{mJ/m}^2$ for the AFM. The effect of finite temperature is not considered in the results discussed above due partly to the fact that stable formation of magnetic skyrmions has already been observed experimentally in the FM systems at room temperature [13, 38]. As for the AFM structures, our stochastic simulations based on the Gaussian-distributed random thermal fluctuations in the effective field also suggest no major impact on the skyrmion writing/deleting process described in Fig. 2 up to 300 K, indicating the stability of AFM skyrmion in the case shown. A comprehensive account of the random thermal effect is not attempted in this work.

Following the cases indicating the feasibility, it is important to examine the conditions necessary for stable skyrmion formation in the relevant parameter space for a more systematic understanding (thus, without K_{pma}). Equations (1) and (2) indicate that to minimize the total energy in either the FM or AFM, the exchange interaction tends to align the mag-

netization parallel (or antiparallel) to its neighbor while the DMI leads the magnetization to be perpendicular to each other. The anisotropy term reduces the total energy when m_z increases (for $K > 0$). Clearly the equilibrium state of the system is constrained by D, A, and K [39, 40]. It has been shown that the range of D for individual skyrmion creation is limited by A and K with the critical value given as at zero temperature [41]

$$D_c = \frac{4(AK)^{1/2}}{\pi}. \tag{3}$$

Here, K corresponds to K_z and only the absolute magnitude is considered for D and A. The heterostructure environment assumed in the current analysis offers a possibility to separately tailor these parameters in the implementation. For instance, the magnetic anisotropy (K) in a thin film can be substantially modified by the external factors such as the film thickness and the strain with the substrate [30, 42]. Similarly, the strength of the DMI (D) can be controlled through the choice of the spin-orbit coupled material as it is associated with the interaction at the interface [39].

Based on the numerical calculation in the considered structures, we examine the parameter space where the individual skyrmion phase exists as an equilibrium state. Figure 3 provides the results of the parametric analysis. The ranges of the relevant values are chosen according to those reported in the literature (see, for instance, Refs. [12] and [43] for A and D, respectively. Identical conditions are assumed for both the FM and AFM systems for a direct comparison. As shown, $D \approx D_c$ in fact appears to be ideal for formation of the desired nanoscale topological solitons. Outside the rather narrow range, region 1 allows only the ground state in the FM (AFM) phase, respectively, whereas multi-domains form in region 2 that cannot hold a single compact skyrmion. Note that the conditions leading to an extended skyrmions or a bimeron (i.e., near the boundary with the colored area) are conveniently classified into region 2 since they are not as desirable in the applications. As for the edges with region 1, the possibility of individual metastable skyrmions (instead of the stable ones) exists [44]. The difference between the two is not readily identifiable in the current analysis if, in particular, the lifetime of the metastable state is orders of magnitude longer than the typical duration of the simulation (around 10's of ns and 100's of ps for the FM and AFM structures, respectively).

In the parameter space where the system has two stable states, each phase [i.e., FM (AFM) and skrymion] corresponds to an energy minimum with an energy barrier between

them. An increase in the anisotropy energy via the induced PMA (i.e., $K_{\mathrm{pma}} < 0$) drives the system away from equilibrium and rotates magnetization toward a lower energy configuration. When this perturbation is turned off, the spin textures relax to a phase closest to the present state. If the instantaneous state is more "skyrmionic", the textures will settle to an individual skyrmion eventually. On the other hand, the spin structure in the film returns to the initial FM (AFM) phase when the excitation is insufficient to overcome the barrier. The dynamics of destruction can be understood from Fig. 3 as well. By effectively increasing K_z through a positive K_{pma} while keeping other parameters constant, the skyrmion phase is no longer a stable state and the system moves to region 1 with the ground state in the FM (AFM) phase. In this case, the skyrmion shrinks in size and eventually disappears. Due to the presence of energy barrier even without K_{pma}, it cannot spontaneously switch back to the skyrmion state after destruction. During this process, the magnetization (or the Néel vector) at the core experiences opposite reversal from $-\hat{\mathbf{z}}$ to $+\hat{\mathbf{z}}$. The duration of the destruction bias can be much shorter than that for generation particularly in the FM case. This is because the exchange interaction at the skyrmion boundary becomes dominant as its size is reduced and can quickly settle the spin textures to the FM phase.

As for the comparison between the FM and AFM cases, the dynamics for both formation and dissolution are much faster in the AFMs as discussed earlier (e.g., ~10 ps vs. ~1 ns for skyrmion creation). The main origin of this speed-up is the absence of precessional motion that can be seen clearly from in Fig. 4(a,b). The dominant AFM exchange field restricts the magnetizations of the two sublattices (A,B) to be always antiparallel to each other. Accordingly, the reversal process is achieved in a pendulum-like fashion essentially on a 2D plane without much in-plane motion [22]. In contrast, the FM magnetization with no such constraint takes a 3D trajectory. The unnecessary in-plane rotation results in expansion and contraction of the affected area in the magnetic film, significantly prolonging the process.

Faster dynamics also means that the necessary pulse duration Δt can be much shorter for the AFM skyrmions. Figure 4(c) shows the calculated minimum pulse duration Δt_c to complete the creation process. This threshold value is clearly dependent on the magnitude of K_{pma}. The induced torque must be long and strong enough to ensure nearly 180° reversal in some part of the magnetic film by overcoming the existing anisotropy K_z. The issue of Δt_c (thus, K_{pma}) is more crucial to the FM skyrmion in the practical applications as the characteristic time for the AFM case is already short in the ps range. As shown, Δt_c

starts to go up rather drastically at around $-250\,\mathrm{kJ/m^3}$ (AFM) or $-300\,\mathrm{kJ/m^3}$ (FM) with the decreasing PMA strength. These points may represent the practical lower bound for the desired anisotropy modulation given the anisotropy values of the magnet used in the calculation ($K_z = 200\,\mathrm{kJ/m^3}$, $K_x=K_y=0$). The observed deviation between lines 1 and 2 can be attributed to the different sizes of the skyrmions in the respective cases in reference the the gate electrode dimension. Our simulation results indicate that the formation process tends to settle faster when the anisotropy modulation is introduced in a broader region blanketing entirely the emergent skyrmion and its vicinity. As the parameters used for line 1 leads to a larger skyrmion, the coverage by a fixed sized gate is relatively not as complete, necessitating a longer excitation pulse for the desired "skyrmionic" textures. This dependence (on the relative size) manifests itself when the signal strength is reduced. In comparison, a sufficient change in the magnetic anisotropy can keep the necessary pulse duration around 100 ps or possibly shorter in the FM system even for the parameter values outside the currently considered range (for instance, those adopted for PdFe/Ir(111) [45]). A recent experiment suggests that the anisotropy modulation in the range of 300-400 $\mathrm{kJ/m^3}$ can be within reach via VCMA [30]. The magnetoelastic effect is expected to be effective as well [37]. To stay within the realizable pulse strength, it may also be desirable to use a magnetic material with low magnetocrystalline anisotropy [46] and further tailor the properties via extrinsic conditions available to the thin-film geometry for a small effective barrier K_z (see, for instance, Refs. [42] and [47]).

Although FM skyrmions are at a disadvantage in terms of the speed, they exhibit better stability. If overwrite occurs, i.e., a creation voltage is applied to an already existing skyrmion, the FM one experiences perturbation but soon recovers. In contrast, the spin textures on an AFM film can be disturbed more significantly and may become a multi-domain structure. One potential remedy may be to ensure that no skyrmion exists before applying a creation pulse. The additional step for the reset would require a destruction sequence ahead of any "writing" (either "1" or "0"). Due to the short overhead for this process ($\lesssim 2$ ps), the overall operation of the device based on AFM skyrmions is not expected to be delayed significantly.

Finally, it is interesting to consider the non-ideal case of $K_x \neq K_y$. Due to the intrinsic and extrinsic factors such as the shape anisotropy, it is not unlikely to encounter inhomogeneous in-plane anisotropy in a magnetic nanostrip such as that shown in Fig. 1. To account for this

possibility, non-zero K_y is introduced to the calculation. Specifically, the magnetic film is still characterized by the z-directional easy axis with $K_z = 200 \text{ kJ/m}^3$ and $K_x = 0$ while K_y is varied from -50 kJ/m^3 to 50 kJ/m^3. Then the anisotropy energy term in the Hamiltonian expression needs to be modified slightly as:

$$H_{an} = -K_y \sum_i m_{i,y}^2 - K_z \sum_i m_{i,z}^2. \tag{4}$$

The conditions for K_{pma} remains the same as before. Figure 5 summarizes the simulation results for the generation process. When K_y is somewhat negative (thus, making the y direction a bit hard), a stable skyrmion can be excited as before in both FM and AFM structures. If any, this condition may be slightly more advantageous than the homogeneous case ($K_x = K_y = 0$) as the size appears to be smaller. Even when K_y becomes slightly positive (thus, competing with the z direction), the applied PMA pulse leads to the successful excitation. However, once this component becomes substantial (thus, a secondary easy axis), the stable textures take an elongated shape (i.e., bimeron-type). The elongation pattern along with a larger size can be understood from Fig. 3(c,d). As the anisotropy along the easy z-axis is effectively weakened, the system tends to have more multi-domain character (region 2). Such an effect may be partly mitigated if other parameters (such as A and D) are adjusted properly. As for the destruction, the skyrmions can be dissolved similarly with a positive PMA pulse despite the changes. One potential complication is that the size of the gate contact may need to be increased substantially to cover most, if not all, of the extended spin textures. The characteristic speed for deletion also becomes slower with a positive K_y. The skyrmion generation time, on the other hand, appears to be largely unaffected by the inhomogeneous in-plane anisotropy. Needless to mention, the observed sensitive dependence of the characteristic skyrmion features on the magnetic anisotropy profile makes it crucial to maintain the uniformity of this property throughout the film in the active device. For instance, the resulting variation in the skyrmion sizes can lead to disparate speeds of motion under the same driving current, posing a potentially significant limiting factor in the performance of the proposed racetrack-type structures.

IV. SUMMARY

A currentless method for creation and destruction of individual Néel-type skyrmion is theoretically examined. Local magnetization rotation induced by electrical modulation of magnetic anisotropy from easy axis to easy plane is shown to realize skyrmion formation in both FM and AFM thin films with judicious selection of materials and operating conditions. Likewise, the destruction can be achieved by enhancing the PMA in the region that supports the topologically protected spin textures. The dynamical processes involved are much faster in the AFMs particularly for the excitation due to the dominant AFM coupling between sublattices (e.g., $\sim$10 ps vs. $\sim$1 ns). The destruction appears to require substantially less time than the generation. The size of individual skyrmion can be scaled down to the sub-10 nm range in the radius without sacrificing the stability by properly selecting the relevant material and interaction parameters. The simulation results also indicate the robustness against a small inhomogeneity in the in-plane magnetic anisotropy profile. Considering the low power and locally controlled nature of magnetic anisotropy modulation, this approach is expected to provide a highly efficient means to encode logic information in the skyrmion based structures for device applications. The AFMs offer a particularly promising opportunity for their speed.

[1] T. H. R. Skyrme, A unified field theory of mesons and baryons, Nucl. Phys. **31**, 556 (1962).

[2] A. N. Bogdanov and U. K. Rößler, Chiral symmetry breaking in magnetic thin films and multilayers, Phys. Rev. Lett. **87**, 037203 (2001).

[3] X. Xing, P. W. Pong, and Y. Zhou, Skyrmion domain wall collision and domain wall-gated skyrmion logic, Phys. Rev. B **94**, 054408 (2016).

[4] X. Zhang, M. Ezawa, and Y. Zhou, Magnetic skyrmion logic gates: Conversion, duplication and merging of skyrmions, Sci. Rep. **5**, 9400 (2015).

[5] D. A. Garanin, D. Capic, S. Zhang, X. Zhang, and E. M. Chudnovsky, Writing skyrmions with a magnetic dipole, arXiv:1806.06393.

[6] W. Koshibae and N. Naoto, Creation of skyrmions and antiskyrmions by local heating, Nat. Commun. **5**, 5148 (2014).

[7] G. Berruto, I. Madan, Y. Murooka, G. M. Vanacore, E. Pomarico, J. Rajeswari, R. Lamb, P. Huang, A. J. Kruchkov, Y. Togawa, T. LaGrange, D. McGrouther, H. M. Rønow, and F. Carbone, Laser-induced skyrmion writing and erasing in an ultrafast cryo-Lorentz transmission electron microscope, Phys. Rev. Lett. **120**, 117201 (2018).

[8] C. Jin, C. Song, J. Wang, and Q. Liu, Dynamics of antiferromagnetic skyrmion driven by the spin Hall effect, Appl. Phys. Lett. **109**, 182404 (2016).

[9] N. Romming, C. Hanneken, M. Menzel, J. E. Bickel, B. Wolter, K. von Bergmann, A. Kubetzka, and R. Wiesendanger, Writing and deleting single magnetic skyrmions, Science **341**, 636 (2013).

[10] J. Sampaio, V. Cros, S. Rohart, A. Thiaville, and A. Fert, Nucleation, stability and current-induced motion of isolated magnetic skyrmions in nanostructures, Nat. Nanotechnol. **8**, 839 (2013).

[11] W. Jiang, P. Upadhyaya, W. Zhang, G. Yu, M. B. Jungfleisch, F. Y. Fradin, J. E. Pearson, Y. Tserkovnyak, K. L. Wang, O. Heinonen, S. G. E. te Velthuis, and A. Hoffmann, Blowing magnetic skyrmion bubbles, Science **349**, 283 (2015).

[12] X. Zhang, Y. Zhou, and M. Ezawa, Antiferromagnetic skyrmion: Stability, creation and manipulation, Sci. Rep. **6**, 24795 (2016).

[13] G. Yu, P. Upadhyaya, Q. Shao, H. Wu, G. Yin, X. Li, C. He, W. Jiang, X. Han, P. K. Amiri,

and K. L. Wang, Room-temperature skyrmion shift device for memory application, Nano Lett. **17**, 261 (2017).

[14] X. Zhang, M. Ezawa, D. Xiao, G. P. Zhao, Y. Liu, and Y. Zhou, All-magnetic control of skyrmions in nanowires by a spin wave, Nanotechnol. **26**, 225701 (2015).

[15] Y. Zheng, and Y. Wang, Continuous nucleation dynamics of magnetic skyrmions in T-shaped helimagnetic nanojunction, arXiv:1804.04022.

[16] S. Z. Lin, Edge instability in a chiral stripe domain under an electric current and skyrmion generation, Phys. Rev. B **94**, 020402 (2016).

[17] B. Göbel, A. Mook, J. Henk, and I. Mertig, Antiferromagnetic skyrmion crystals: Generation, topological Hall, and topological spin Hall effect, Phys. Rev. B **96**, 060406 (2017).

[18] Y. Shi, and J. Wang, Stabilizing skyrmions by nonuniform strain in ferromagnetic thin films without a magnetic field, Phys. Rev. B **97**, 224428 (2018).

[19] T. Maruyama, Y. Shiota, T. Nozaki, K. Ohta, N. Toda, M. Mizuguchi, A. A. Tulapurkar, T. Shinjo, M. Shiraishi, S. Mizukami, Y. Ando, and Y. Suzuki, Large voltage-induced magnetic anisotropy change in a few atomic layers of iron, Nat. Nanotechnol. **4**, 158 (2009).

[20] P. K. Amiri and K. L. Wang, Voltage-controlled magnetic anisotropy in spintronic devices, Spin **2**, 1240002 (2012).

[21] W. Kang, Y. Ran, Y. Zhang, W. Lv, and W. Zhao, Modeling and exploration of the voltage-controlled magnetic anisotropy effect for the next-generation low-power and high-speed MRAM applications, IEEE Trans. Nanotechnol. **16**, 387 (2017).

[22] Y. G. Semenov, X. L. Li, and K. W. Kim, Currentless reversal of Néel vector in antiferromagnets, Phys. Rev. B **95**, 014434 (2017).

[23] W. Kang, Y. Huang, C. Zheng, W. Lv, N. Lei, Y. Zhang, X. Zhang, Y. Zhou, and W. Zhao, Voltage controlled magnetic skyrmion motion for racetrack memory, Sci. Rep. **6**, 23164 (2016).

[24] H. Xia, C. Song, C. Jin, J. Wang, J. Wang, and Q. Liu, Skyrmion motion driven by the gradient of voltage-controlled magnetic anisotropy, J. Magn. Magn. Mater. **458**, 57 (2018).

[25] X. Wang, W. L. Gan, J. C. Martinez, F. N. Tan, M. B. A. Jalil, and W. S. Lew, Efficient skyrmion transport mediated by a voltage controlled magnetic anisotropy gradient, Nanoscale **10**, 733 (2018).

[26] D. Bhattacharya, M. M. Al-Rashid, and J. Atulasimha, Voltage controlled core reversal of fixed magnetic skyrmions without a magnetic field, Sci. Rep. **6**, 31272 (2016).

[27] S. Peng, X. Li, W. Kang, H. Zhang, L. Wang, Z. Wang, Z. Wang, Y. Zhang, K. L. Wang, and W. Zhao, Field-free switching of perpendicular magnetic tunnel junction via voltage-gated spin Hall effect for low-power spintronic memory, arXiv:1804.11025.

[28] T. Nozaki, A. Kozioł-Rachwał, W. Skowroński, V. Zayets, Y. Shiota, S. Tamaru, H. Kubota, A. Fukushima, S. Yuasa, and Y. Suzuki, Large voltage-induced changes in the perpendicular magnetic anisotropy of an MgO-based tunnel junction with an ultrathin Fe layer, Phys. Rev. Appl. **5**, 044006 (2016).

[29] J. G. Alzate, P. K. Amiri, G. Yu, P. Upadhyaya, J. A. Katine, J. Langer, B. Ocker, I. N. Krivorotov, and K. L. Wang, Temperature dependence of the voltage-controlled perpendicular anisotropy in nanoscale MgO|CoFeB|Ta magnetic tunnel junctions, Appl. Phys. Lett. **104**, 112410 (2014).

[30] T. Nozaki, A. Kozioł-Rachwał, M. Tsujikawa, Y. Shiota, X. Xu, T. Ohkubo, T. Tsukahara, S. Miwa, M. Suzuki, S. Tamaru, H. Kubota, A. Fukushima, K. Hono, M. Shirai, Y. Suzuki, and S. Yuasa, Highly efficient voltage control of spin and enhanced interfacial perpendicular magnetic anisotropy in iridium-doped Fe/MgO magnetic tunnel junctions, NPG Asia Mater. **9**, e451 (2017).

[31] M. J. Donahue and D. G. Porter, OOMMF User's Guide, Version 1.0 (NIST, Gaithersburg, MD, 1999).

[32] S. S. P. Parkin, M. Hayashi, and L. Thomas, Magnetic domain-wall racetrack memory, Science **320**, 190 (2008).

[33] S. Zhang, A. A. Baker, S. Komineas, and T. Hesjedal, Topological computation based on direct magnetic logic communication, Sci. Rep. **5**, 15773 (2015).

[34] J. Iwasaki, M. Mochizuki, and N. Nagaosa, Current-induced skyrmion dynamics in constricted geometries, Nat. Nanotechnol. **8**, 742 (2013).

[35] J. Barker and O. A. Tretiakov, Static and dynamical properties of antiferromagnetic skyrmions in the presence of applied current and temperature, Phys. Rev. Lett. **116**, 147203 (2016).

[36] C. Hanneken, F. Otte, A. Kubetzka, B. Dupé, N. Romming, K. von Bergmann, R. Wiesendanger, and S. Heinze, Electrical detection of magnetic skyrmions by tunnelling non-collinear magnetoresistance, Nat. Nanotechnol. **10**, 1039 (2015).

[37] See, for instance, M. Gueye, F. Zighem, M. Belmeguenai, M. S. Gabor, C. Tiusan, and D. Faurie, Effective 90-degree magnetization rotation in Co_2FeAl thin film/piezoelectric system

probed by microstripline ferromagnetic resonance, Appl. Phys. Lett. 107, 032908 (2015).

[38] C. Moreau-Luchaire, C. Moutafis, N. Reyren, J. Sampaio, C. A. F. Vaz, N. Van Horne, K. Bouzehouane, K. Garcia1, C. Deranlot, P. Warnicke, P. Wohlhter, J.-M. George, M. Weigand, J. Raabe, V. Cros, and A. Fert, Additive interfacial chiral interaction in multilayers for stabilization of small individual skyrmions at room temperature, Nat. Nanotechnol. 11, 444 (2016).

[39] A. Fert, N. Reyren, and V. Cros, Magnetic skyrmions: Advances in physics and potential applications, Nat. Rev. Mater. 2, 17031 (2017).

[40] Y. Zhou, E. Iacocca, A. A. Awad, R. K. Dumas, F. C. Zhang, H. B. Braun, and J. Åkerman, Dynamically stabilized magnetic skyrmions, Nat. Commun. 6, 8193 (2015).

[41] S. Rohart and A. Thiaville, Skyrmion confinement in ultrathin film nanostructures in the presence of Dzyaloshinskii-Moriya interaction, Phys. Rev. B 88, 184422 (2013).

[42] P. G. Gowtham, G. M. Stiehl, D. C. Ralph, and R. A. Buhrman, Thickness-dependent magnetoelasticity and its effects on perpendicular magnetic anisotropy in Ta/CoFeB/MgO thin films, Phys. Rev. B 93, 024404 (2016).

[43] A. Hrabec, N. A. Porter, A. Wells, M. J. Benitez, G. Burnell, S. McVitie, D. McGrouther, T. A. Moore, and C. H. Marrows. Measuring and tailoring the Dzyaloshinskii-Moriya interaction in perpendicularly magnetized thin films, Phys. Rev. B 90, 020402 (2014).

[44] A. Soumyanarayanan, M. Raju, A. L. Gonzalez Oyarce, A. K. C. Tan, M.-Y. Im, A. P. Petrović, P. Ho, K. H. Khoo, M. Tran, C. K. Gan, F. Ernult, and C. Panagopoulos, Tunable room-temperature magnetic skyrmions in Ir/Fe/Co/Pt multilayers, Nat. Mater. 16, 898 (2017).

[45] N. Romming, A. Kubetzka, C. Hanneken, K. von Bergmann, and R. Wiesendanger, Field-dependent size and shape of single magnetic skyrmions, Phys. Rev. Lett. 114, 177203 (2015).

[46] A. Barra, J. Domann, K. W. Kim, and G. Carman, Voltage control of antiferromagnetic phases at near-terahertz frequencies, Phys. Rev. Applied 9, 034017 (2018).

[47] H. V. Gomonay and V. M. Loktev, Shape-induced phenomena in finite-size antiferromagnets, Phys. Rev. B 75, 174439 (2007).
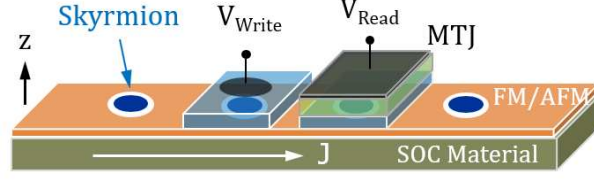
FIG. 1: Schematic illustration of a racetrack-like magnetic structure. The information can be written on the skyrmion, which can then be transferred or stored along the channel via the electrical current J in a strongly spin-orbit coupled (SOC) material. An individual Skyrmion can be generated and destroyed in the magnetic thin film (logic "1" and "0") via bias induced magnetic anisotropy under the gate. A MTJ can be used for read-out.
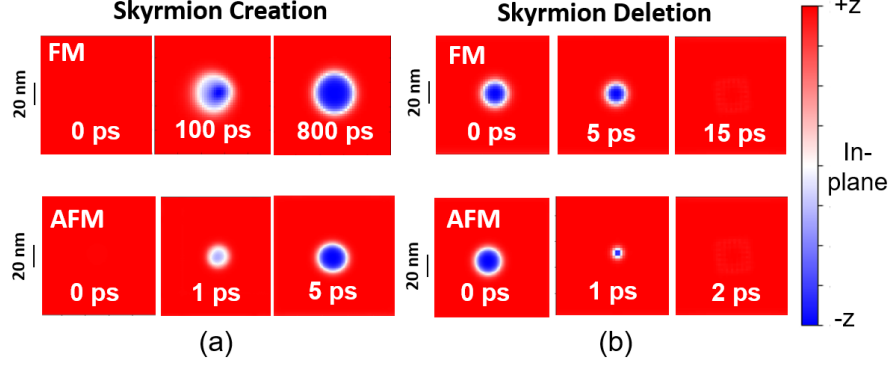
FIG. 2: Snapshots of the simulated spin texture evolution in both FM and AFM films, highlighting (a) skyrmion formation and (b) dissolution. For creation, a PMA pulse with $K_{\text{pma}} = -400$ kJ/m^3 is applied for the duration Δt of 100 ps and 1 ps for the FM and AFM cases, respectively. The destruction process assumes $K_{\text{pma}} = +100$ kJ/m^3 with Δt of 20 ps (FM) and 2 ps (AFM), respectively. The exchange stiffness and DMI constants are set to $A = 5$ pJ/m, $D = 1.2$ mJ/m^2 (FM) and $A = -3$ pJ/m, $D = -0.9$ mJ/m^2 (AFM). The easy z-axis anisotropy of $K_z = 200$ kJ/m^3 is used in all cases.
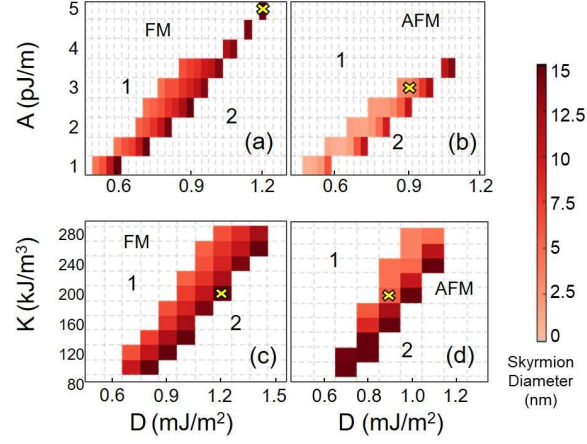
FIG. 3: Parameter space for stable skyrmions. In (a,b), the easy z-axis anisotropy is fixed at $K_z = 200$ kJ/m^3, whereas in (c,d) a constant value is for the exchange stiffness $A = 5$ pJ/m. Region 1 represents the conditions, where the system ground state is the (a,c) FM or the (b,d) AFM phase, respectively. In contrast, the multi-domain phase is the energetically stable state in region 2. Finally, the shaded or colored regions are where the system supports two stable states (thus, skyrmion formation). The color code indicates the size of stable skyrmions and the cross symbols correspond to the parameter values used in Fig. 2.
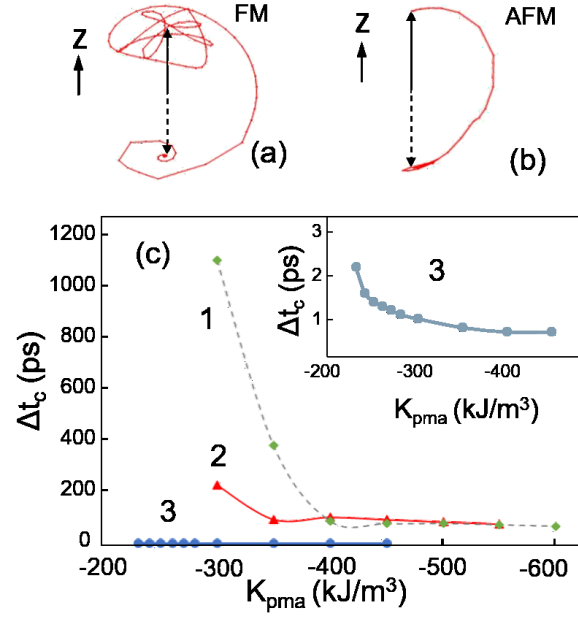
FIG. 4: Characteristic magnetization or Néel vector dynamics at the skyrmion core in the creation process; (a) FM skyrmion and (b) AFM skyrmion. The solid and dashed arrows represent the $+\hat{\mathbf{z}}$ and $-\hat{\mathbf{z}}$ orientations, respectively. (c) Minimum PMA pulse duration Δt_c for skyrmion creation vs. pulse strength K_{pma} with $K_z = 200$ kJ/m^3. Lines 1 and 2 are for the FM with $D = 1.2$ mJ/m^2, $A = 5$ pJ/m and $D = 0.95$ mJ/m^2, $A = 3$ pJ/m, respectively. Line 3 shows the result for the AFM skyrmion with $D = -0.9$ mJ/m^2, $A = -3$ pJ/m. The inset provides a magnified view of line 3.
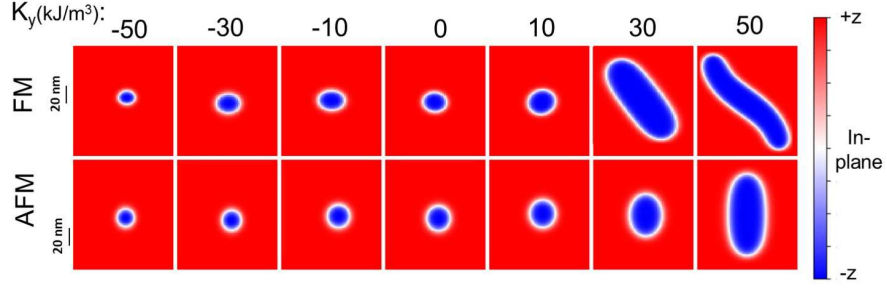
FIG. 5: Skyrmion generation with inhomogeneous in-plane magnetic anisotropy. The magnetic films are characterized by $K_z = 200$ kJ/m^3 and $K_x = 0$ as before but K_y is now varied between -50 kJ/m^3 to 50 kJ/m^3. Other conditions are as specified in Fig. 2.